INTERNATIONAL JOURNAL FOR NUMERICAL METHODS IN FLUIDS, VOL. 14, 443–457 (1992)

PERIODIC SOLUTION OF TURBULENT OSCILLATING CHANNEL FLOWS

QIN ZHONG AND M. D. OLSON

Department of Civil Engineering, University of British Columbia, Vancouver, BC, Canada V6T 1W5

SUMMARY

The time-dependent turbulent Navier–Stokes equations are solved numerically by a finite element method with an algebraic eddy viscosity model (Baldwin–Lomax formulation) for oscillating turbulent channel flows. The method of averaging is used to analyse the resulting periodic motion of the fluid. Numerical results are obtained for various Strouhal numbers and relative amplitudes. A comparison is made between the numerical and published experimental results. It appears that for low relative amplitudes in a certain range of frequencies the agreement is satisfactory.

KEY WORDS Turbulent oscillating flows Finite element method The method of averaging

1. INTRODUCTION

It is very important to take into account the effects of flow unsteadiness for many practical applications in aerodynamic and coastal engineering. Much work has already been devoted to unsteady laminar flow situations and the area is well understood. However, for the turbulent case, results are less abundant and consequently the knowledge of this problem is relatively poor.

The earlier experimental study of an oscillating turbulent boundary layer was carried out in 1959 by Karlsson,[1] who measured the mean properties and the harmonic component under a wide range of free stream amplitudes and oscillation frequencies. He found that the mean characteristics of the boundary layer are not much different from those of the steady state case. Cousteix *et al.*[2] investigated an unsteady turbulent boundary layer in the presence of an oscillatory free stream. The experimental observations showed that the general behaviour of the boundary layer and the structure of the turbulence are not fundamentally affected by the unsteadiness of the flow. An experimental investigation of the periodic velocity oscillations in unsteady turbulent channel flow by Binder and Kueny[3] confirmed the previously published results. The mean velocity profiles measured in oscillating flow are indistinguishable from those in steady flow in a certain range of frequencies. From these observations it is well founded to suppose that the hypotheses used in calculation methods for the steady case are still valid for the unsteady case. A compilation of unsteady turbulent boundary layer experimental data was made by Carr.[4]

In the analysis area, several turbulent closures developed for steady flows have been applied to unsteady flows. Telionis and Tsahalis[5] considered time-dependent turbulent flows over a semi-infinite plate. The boundary layer equations were integrated numerically with the Cebeci–Smith eddy viscosity model used for closure. Extensive comparisons with experimental data were

0271–2091/92/040443–15$07.50

Received 11 October 1990
Revised 28 May 1991

attempted for the first time. Cousteix *et al.*[2] studied the structure and development of a turbulent boundary layer in an oscillatory external flow. A classical mixing length model and a two-equation turbulence closure model were used in the numerical prediction. The numerical results indicated that both turbulence models seemed to be valid for unsteady flow. Telionis[6] gave a detailed review of unsteady boundary layer work. All the existing analytical models were carried over from steady flow and it was argued that for some methods the agreement between the numerical results and experimental data was imperfect but probably adequate for engineering purposes. Some more recent studies are presented in References 7 and 8. In all the foregoing modelling work the transient equations were integrated numerically in time.

In the present paper the need for this numerical integration in time is eliminated by assuming the solution to be periodic and applying the method of averaging. To the writers' knowledge this is the first time this approach has been applied to turbulent flow calculations. The Navier–Stokes equations incorporating the Baldwin–Lomax eddy viscosity model are discretized by the use of the finite element method. The calculation methods developed previously for periodically oscillating laminar flow and steady turbulent flow[9,10] are appropriately extended to periodically oscillating turbulent flow.

An approximation is introduced in the present study in order to simplify the calculations. That is, the eddy viscosity is frozen at the level calculated from the mean component of the flow. This approximation was severely criticized by one of the reviewers with, we must agree, some justification. However, the significance of this approximation cannot be determined until a more rigorous analysis is carried out or results from other methods become available. The current method is applied to a few cases for which experimental results are available and in most cases reasonable comparisons are observed.

2. GOVERNING EQUATIONS AND METHOD OF SOLUTION

For two-dimensional incompressible, unsteady, turbulent flow the Navier–Stokes equations incorporating an eddy viscosity model are given by

$$\begin{aligned} \rho(u_{,t} + uu_{,x} + vu_{,y}) &= -p_{,x} + 2(\mu_e u_{,x})_{,x} + [\mu_e(v_{,x} + u_{,y})]_{,y}, \\ \rho(v_{,t} + uv_{,x} + vv_{,y}) &= -p_{,y} + 2(\mu_e v_{,y})_{,y} + [\mu_e(v_{,x} + u_{,y})]_{,x}, \\ u_{,x} + v_{,y} &= 0, \end{aligned} \tag{1}$$

where x and y are the co-ordinates and u and v are the ensemble-averaged velocity components respectively, t is the time, ρ is the density, p is the pressure and μ_e is the effective viscosity made up of the molecular viscosity μ and the eddy viscosity μ_t.

The present work uses curved isoparametric elements with biquadratic interpolation for velocity and bilinear for pressure. The velocities and pressure are represented by

$$\begin{aligned} u &= N_i u_i(t), \qquad i = 1, 2, \ldots, 8, \\ v &= N_i v_i(t), \qquad i = 1, 2, \ldots, 8, \\ p &= M_i p_i(t), \qquad i = 1, 2, 3, 4, \end{aligned} \tag{2}$$

where N_i and M_i are the shape functions and u_i, v_i and p_i are the time-dependent nodal variables.

The interpolation functions (2) are substituted into equations (1) and the method of weighted residuals is employed to generate the finite element equations

$$\mathbf{M}\dot{\mathbf{d}} + \mathbf{K}\mathbf{d} + \boldsymbol{\delta} = 0, \tag{3}$$

where $\mathbf{M}$ is the mass matrix, $\mathbf{K}$ is the stiffness matrix, $\boldsymbol{\delta}$ contains the non-linear terms due to the

convection terms in equations (1) and **d** is the nodal vector of unknowns u, v and p. Further details are available in Reference 9.

The direct solution of the resulting finite element equations (3) is time-consuming and expensive. In the present study a periodic solution is desired and hence the method of averaging is used to advantage. We assume that the nodal vector of unknowns takes the periodic form

$$\mathbf{d} = \mathbf{A} + \mathbf{B}\cos(\Omega t) + \mathbf{C}\sin(\Omega t), \tag{4}$$

where **A** is a constant vector, the vectors **B** and **C** are assumed to be slowly varying functions of time and Ω is the oscillatory frequency. In equation (4) the nodal vector is composed of a mean component **A** and a harmonic component with in-phase and out-of-phase amplitudes **B** and **C** respectively. When the method of averaging is applied, **B** and **C** are replaced by their average values and $\dot{\mathbf{B}}$ and $\dot{\mathbf{C}}$ are set equal to zero. Thus

$$\dot{\mathbf{d}} = -\mathbf{B}\Omega\sin(\Omega t) + \mathbf{C}\Omega\cos(\Omega t). \tag{5}$$

To obtain the three sets of equations for the three sets of unknowns **A**, **B** and **C**, equations (4) and (5) are first substituted into the finite element equations (3), then the resulting equations are (i) averaged over the period $2\pi/\Omega$, (ii) multiplied by $\sin(\Omega t)$ and averaged over the period $2\pi/\Omega$ and (iii) multiplied by $\cos(\Omega t)$ and averaged over the period $2\pi/\Omega$. Through this process a set of non-linear algebraic equations for **A**, **B** and **C** is obtained. These equations are solved using the Newton–Raphson method following Reference 9. In Reference 9 the method was applied to an extensive number of laminar problems and the predictions were compared with experimental results. It was found to provide excellent predictions for a wide range of Reynolds and Strouhal numbers.

The relaxation technique developed in Reference 10 is employed to calculate the eddy viscosity. A uniform eddy viscosity field is first established from an appropriate laminar solution. The eddy viscosity is held constant while several Newton–Raphson iterations are performed on the velocity–pressure variables. Once the velocity–pressure field has converged, the turbulence models are invoked and the viscosity distribution is updated by the relaxation formulation. Then the velocity–pressure calculations are repeated with the new eddy viscosity distribution. This process is continued until the viscosity has converged as well.

All matrices are evaluated by 3×3 Gauss numerical integration and all the calculations for the turbulent viscosity are carried out at the Gauss points. The computer programmes are implemented in double precision on a new supercomputer system with vector facility (IBM 3090). The solution of the linear algebraic equations and the matrix inversions are performed using a sparse-matrix-solving package called SPARSPAK (University of Waterloo).

3. TURBULENCE MODEL

The Baldwin–Lomax eddy viscosity model[11] has found wide application in the prediction of steady turbulent flows. The present authors have tested this model and found that it is well behaved for attached flows[12] and with appropriate modifications it can reasonably represent separating flows as well.[13] At the first stage of the present work the original Baldwin–Lomax model with slightly changed empirical constants is used. Some of the constants in the original model were set for finite Mach number flows and these were modified slightly to give a better fit for the incompressible case.[10]

A brief summary of the Baldwin–Lomax model follows. The model provides an algebraic representation of the eddy viscosity as a function of y, the co-ordinate normal to a wall. It is subdivided into two functions, namely an inner one close to the wall and an outer one in the outer

flow, in order to approximate the distinctly different mixing phenomena taking place in the respective regions. In the inner region the eddy viscosity is given by

$$(\mu_t)_{\text{inner}} = \rho[k\ y\ D]^2\,|\omega|, \tag{6}$$

where $|\omega|$ is the magnitude of the vorticity, $k=0{\cdot}4$ is the von Karman constant, y is the normal distance from the wall and D is the Van Driest damping factor, which is given by

$$D = 1 - \exp[-y\sqrt{(\rho\tau_w)}/26\mu], \tag{7}$$

with τ_w the wall shear stress. In the outer region the eddy viscosity is given by

$$(\mu_t)_{\text{outer}} = \rho K C_{cp} F_{\text{wake}} F_{\text{kleb}}, \tag{8}$$

where $K=0{\cdot}0168$ is the Clauser constant, C_{cp} is an additional constant which is taken as $1{\cdot}2$ in the present study and

$$F_{\text{wake}} = y_{\max} F_{\max}. \tag{9}$$

The quantities $y_{\max}$ and $F_{\max}$ are determined from the outer function

$$F(y) = y|\omega|D. \tag{10}$$

$F_{\max}$ is the maximum value of $F(y)$ that occurs in a profile and $y_{\max}$ is the value of y at which $F_{\max}$ occurs. In equation (8) the function F_{kleb} is the Klebanoff intermittency factor given by

$$F_{\text{kleb}} = [1 + 5{\cdot}5(C_{\text{kleb}} y/y_{\max})^6]^{-1}. \tag{11}$$

The empirical constant C_{kleb} is chosen to be $0{\cdot}54$ here. The eddy viscosity is switched from the inner to the outer formula at the location where the values from equations (6) and (8) are equal.

In the original Baldwin–Lomax model the flow field was steady and hence the above formulation gave a constant (in time) eddy viscosity. However, in the present work the flow field is unsteady. Hence if we make the normal quasi-steady assumption, then the eddy viscosity becomes unsteady and in particular periodic. It is possible to include this effect in the present method but it would be extremely complex. Hence in the present work we argue that the periodic component of the flow field is relatively small compared to the steady part and thus the change to the eddy viscosity will also be small. Further, it is known that a small change in the eddy viscosity has only a minor effect on the overall flow field. Hence in the present work the vorticity and the wall shear stress in the Baldwin–Lomax formulae are calculated only from the distribution of the mean component of velocity (i.e. part **A** in equation (4)). In the following numerical examples some numerical tests are conducted to check out the effect of these approximations, and indeed they seem to be reasonable.

4. RESULTS AND DISCUSSION

Two flow problems for which experimental data were available are used as test applications herein. These are designated as cases A and B. In case A[3] the measurements were performed in a water channel of length 2600 mm, height 100 mm and span 1000 mm. The oscillating flow was driven by a reciprocating piston. The velocities were measured with a laser velocimeter operating in the fringe mode and the Doppler frequency was measured with a counter.

In case B[2] the experiments were carried out in a wind tunnel and the periodic flow was generated by means of a rotating vane set in the diffuser section downstream of the test section. The development of the boundary layer was studied on the floor of the 100 mm by 110 mm test section and the velocities were measured with hot wire anemometers. The Reynolds numbers

corresponding to these experiments are quite different and therefore provide an extra challenge to the numerical modelling. Unfortunately the time variation of the periodic component was not measured in case A but the authors' discussion implied it was essentially harmonic. In case B it was measured and indeed it was very close to harmonic. Hence the present periodic solution approximation is well supported by the experimental results.

Several preliminary calculations were carried out with a variety of finite element grids. This culminated in the type of grid shown schematically in Figure 1, which was deemed to be adequate for present purposes, which are mainly to show the validity of the present solution approach. The grid incorporates geometric progression in both directions. Note that the vertical and horizontal scales are not equal.

The following boundary conditions were applied (Figure 1):

$$\begin{aligned}
&\text{upstream,} && x = 0: \quad u = u_0, \quad v = 0,\\
&\text{downstream,} && x = L: \quad p = 0, \quad v = 0,\\
&\text{on the wall,} && y = 0: \quad u = 0, \quad v = 0,\\
&\text{on the symmetry line,} && y = h: \quad \tau = 0, \quad v = 0,
\end{aligned}$$

where $u_0 = u_m + u_p$ is the specified velocity made up of a mean component u_m and a harmonic component u_p. Note that in the present formulation the symmetry line boundary condition of zero shear stress is a natural boundary condition which is not satisfied directly but rather is satisfied by the method in the Galerkin sense.

The details of the finite element grids and the computational conditions are given in Tables I and II respectively. Note that the case A calculations were carried out with a second grid (grid II) which had 50% more elements in the y-direction in order to check on mesh sensitivity through

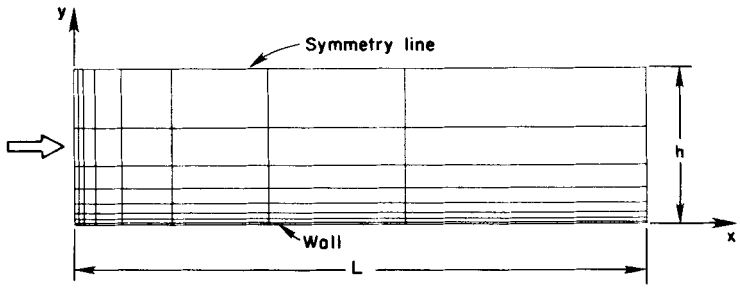

Figure 1. Typical finite element grid and flow domain

Table I. Details of finite element grids

Case	Grid	Number of elements		Element dimensions			
		X	Y	ΔX_{min} (mm)	$\Delta X_i/\Delta X_{i-1}$	ΔY_{min} (mm)	$\Delta Y_i/\Delta Y_{i-1}$
A	I	12	8	4	1·643	0·35	1·814
	II	12	12	4	1·643	0·20	1·495
B		8	8	4	1·9	0·35	1·814

Table II. Computational conditions

Case	Re	St	u_p	u_c (cm s^{-1})	A_c (cm s^{-1})	h (mm)	L (mm)
A	8800	0·133	$A\cos(\Omega t)$	17·5	1·12	50	2400
		1·2	$A\cos(\Omega t)$	17·5	0·98	50	2400
B	67240	0·4	$A\sin(\Omega t)$	3362	1248	50	750

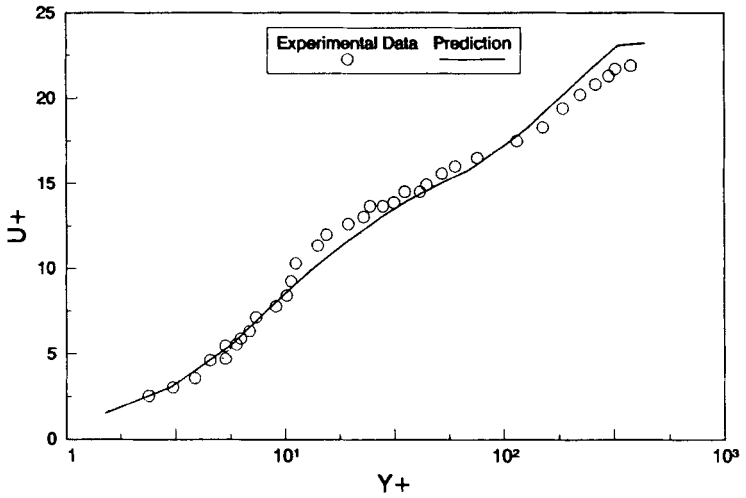

Figure 2. Mean velocity distribution in channel flow (case A)

the boundary layer. Grid refinement in the streamwise direction was not necessary because all the calculated results became fully developed well before the downstream end.

In Table II the Reynolds number Re and the Strouhal number St are based on the half-channel width h and inlet mean velocity u_c at the centre line and A_c is the amplitude of the inlet velocity at the centre line $y = h$.

In case A the relative amplitude of the oscillatory component was small, namely 5·6% and 6·4%. The calculation was performed for two frequencies differing by one order of magnitude, namely $St = 0{\cdot}133$ and 1·2. In the wall region the mean velocity u_m was determined from $\partial u_m/\partial y = 0{\cdot}64\,\rho/\mu$ out to the location where $u_m = u_c$.

The finite element grid I had 96 elements and 329 nodes with 661 net degrees of freedom. Out of the 661, 16 velocity degrees of freedom lie on the upstream boundary and were specified. For the periodic flow situation there are three types of coefficients A, B and C and this resulted in 1935 variables in total. Grid II had 144 elements, 481 nodes and 997 net degrees of freedom with 24 specified velocity components. The final net number of A, B and C variables was then 2919.

Figure 2 shows a comparison of the computed velocity distribution (u^+ versus y^+) from grid I with the experimental data at the location $x = 2400$ mm, where $u^+ = u\sqrt{(\rho/\tau_w)}$ and $y^+ = \sqrt{(\rho\tau_w)}y/\mu$. The grid I and II results are indiscernible from each other at this scale. The mean velocity profiles computed in oscillating flows for two Strouhal numbers are virtually the same as the steady flow curve and are in good agreement with the experimental measurement.[3]

Figures 3 and 4 show the amplitude and phase, respectively, of velocity oscillations in the wall region at a Strouhal number of 1·2 as obtained from both grids. Compared with the experimental data,[3] the present predictions appear to be reasonable. In Figures 5 and 6 the corresponding distributions of the amplitude and phase at $St = 0{\cdot}133$ are presented. The amplitude near the wall follows very closely the experimental data again, but the phase near the wall is quite different from the measurements. The same type of discrepancy was noted in Reference 3 between the experiment and their Stokes flow solution and the authors were not able to explain it. In that sense the present predictions agree with those reported in Reference 3. Some of the present discrepancy may be due to the 'frozen' eddy viscosity approximation used herein. On the other hand, there is qualitative agreement of the present results with those of Karlsson,[1] such as smaller phase shifts

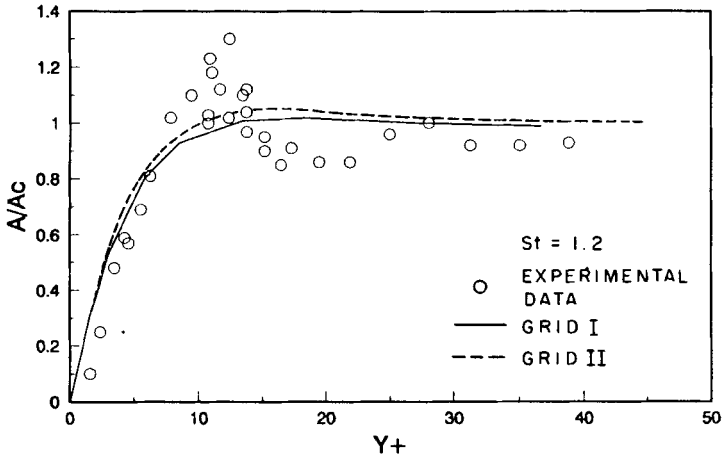

Figure 3. Amplitude in the wall region (case A)

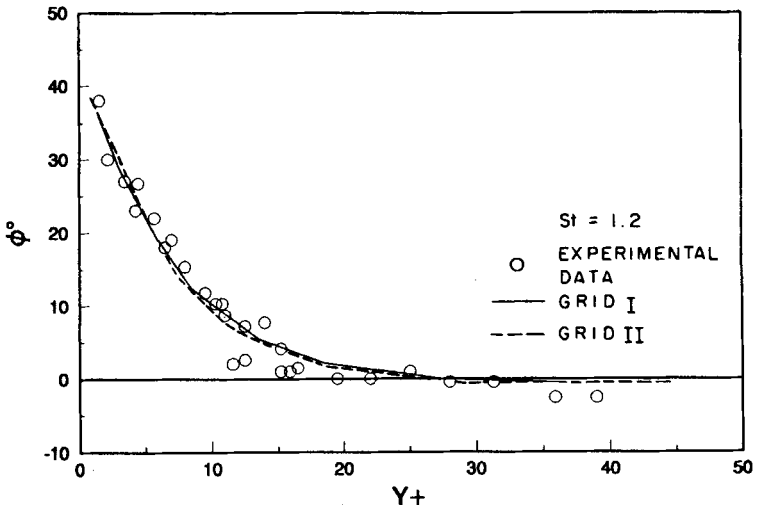

Figure 4. Phase in the wall region (case A)

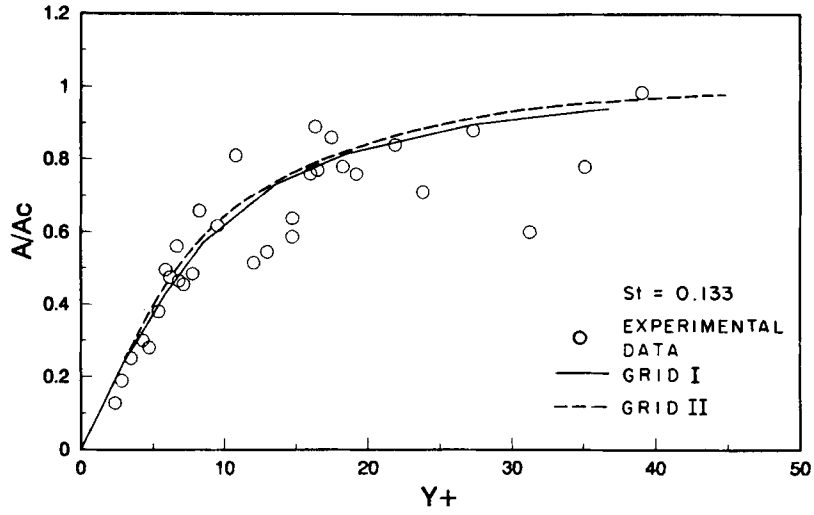

Figure 5. Amplitude in the wall region (case A)

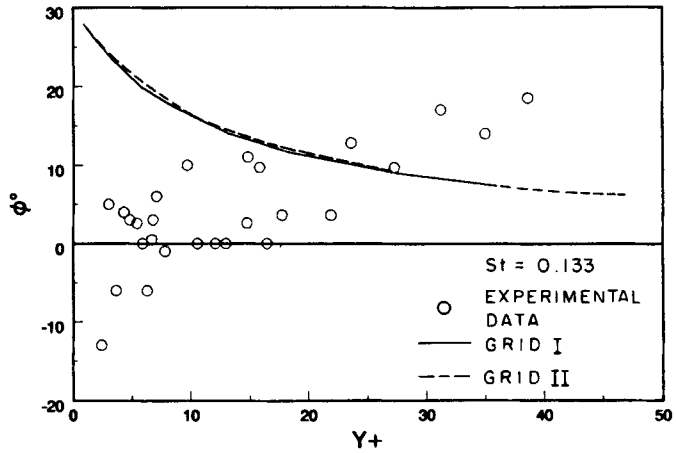

Figure 6. Phase in the wall region (case A)

at lower frequencies. The experimental results appear to be a bit non-physical in that the phase angle does not seem to return to zero far from the wall as it must do.

Finally we note that the grid II results are very close to those from grid I in all four figures and hence we can conclude that the latter grid is adequate for present purposes. However, the finer grid would be needed for more accurate wall quantities such as pressure, friction and heat transfer coefficients, because these quantities depend on derivatives of the velocity field. This has been shown in previous work such as Reference 13.

Some further calculations were carried out to ascertain the effect of neglecting the periodic component in the turbulence modelling. To do this, the amplitudes of the periodic velocity components were added to the steady components wherever the latter occurred in the turbulent

model and the calculations for case A were then repeated. It was felt that this procedure should provide a bound on the real situation where the periodic component is only additive for half of each cycle.

Some typical results of this investigation are shown in Figure 7, where the normalized effective viscosity profiles are plotted with and without the above change. These results are from the central Gauss point in each element at the downstream end of grid II for $St = 1{\cdot}2$. It is seen that very close to the wall the eddy viscosity is negligible and the effective viscosity is just equal to the molecular value. Further out from the wall there is a discernible difference in the two results. The largest relative difference shown here is about 6·5% at $y = 5{\cdot}2$ mm. Coincidentally this difference is close to the relative amplitude of the periodic component for this case, namely 5·6%. The corresponding velocity and phase angle profiles obtained from these calculations when plotted were hardly discernible from those in Figures 3–6. Hence we may conclude from these observations that at least for the low-amplitude situation in case A the neglect of the periodic component in the turbulence model is quite justifiable.

In case B the calculation was performed at a higher relative amplitude of the periodic component, namely 37%. The computational conditions for this case (Table II) correspond to those of the second experiment,[2] but unfortunately the inlet velocity profiles in the wall region were not available from the published experimental results. In order to specify the upstream velocity boundary condition, we solved the same flow configuration with specified uniform inlet velocity profiles first (for both mean and periodic components). Then the computed velocity profiles u_m and A at the location where the displacement thickness δ_1 was nearest to the experimental value at measurement station 1 where $x = 0$ (see Reference 2) were used as the inlet boundary conditions which are shown in Figure 8.

The finite element grid used in this case had 64 elements and 225 nodes with 441 net degrees of freedom. Out of the 441, 16 velocity degrees of freedom lie on the upstream boundary and are specified. For this problem there are 1275 net variables in total.

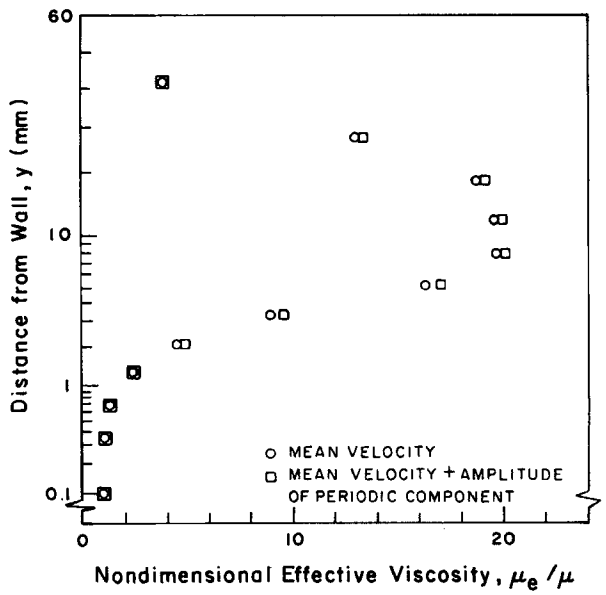

Figure 7. Effect of periodic component on viscosity profiles for case A, $St = 1{\cdot}2$

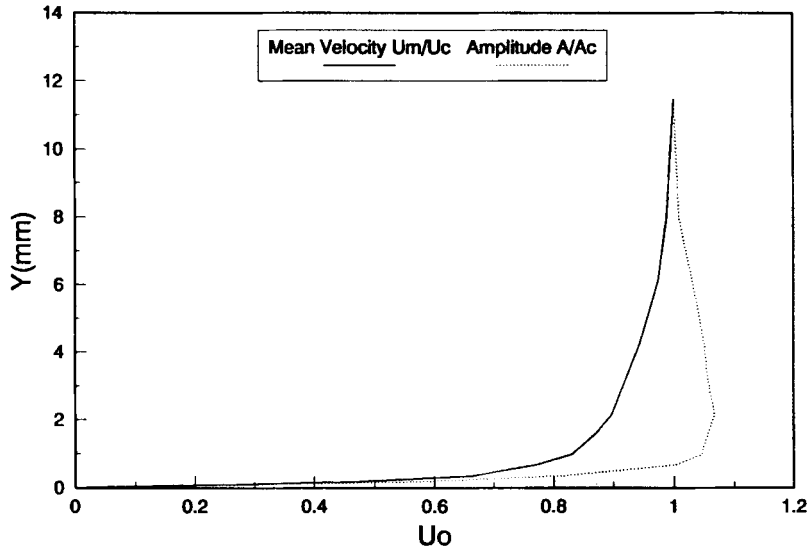

Figure 8. Inlet velocity profiles in the wall region (case B)

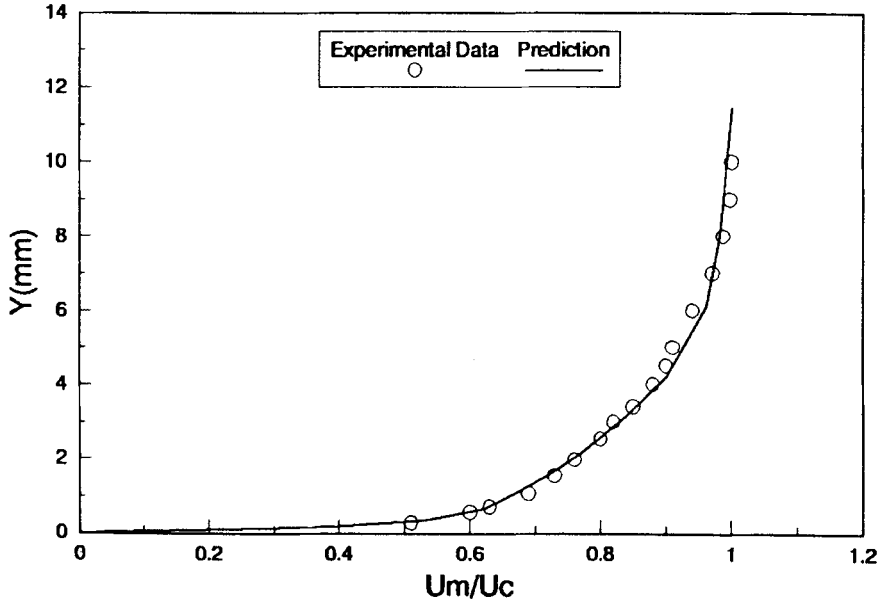

Figure 9. Mean velocity profile in the wall region (case B)

Figures 9 and 10 show the profiles of the mean velocity and the amplitude at the location $x = 210$ mm, which are in good agreement with the experimental measurements.[2] The pattern of the mean velocity profile is very nearly that of the velocity profile for steady flow. Figure 11 shows a comparison of the computed phase with that from the experiment. The computed phase

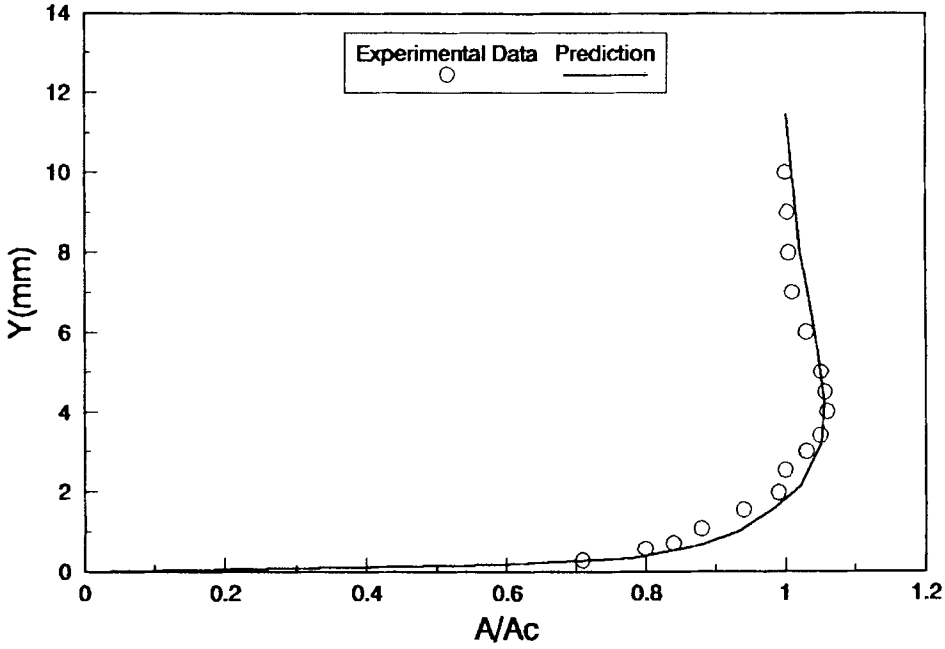

Figure 10. Amplitude in the wall region (case $\bar{B}$)

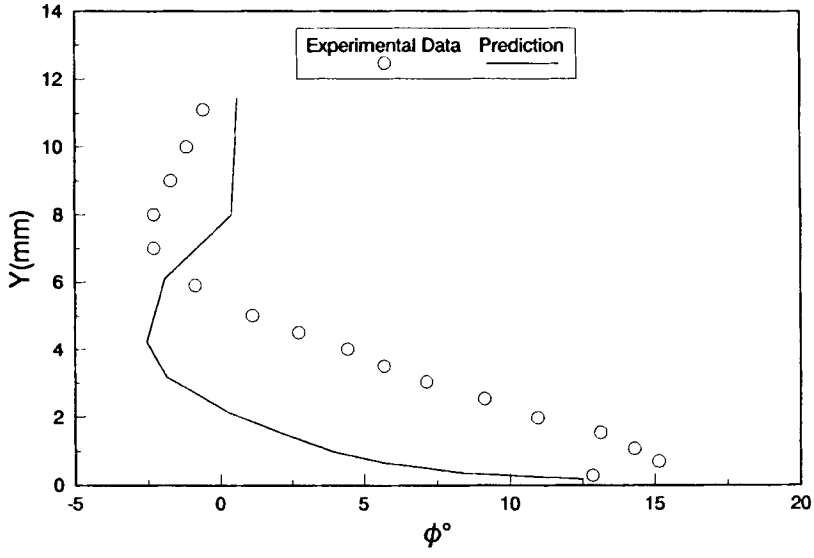

Figure 11. Phase in the wall region (case B)

distribution has the same trend as the experimental measurement but is quite different in magnitude. This latter difference may be due to the inlet conditions, since, as explained before, the experimental conditions were not known and *ad hoc* ones had to be introduced herein. It is also conceivable that for this higher-amplitude case the present turbulence modelling is not optimum.

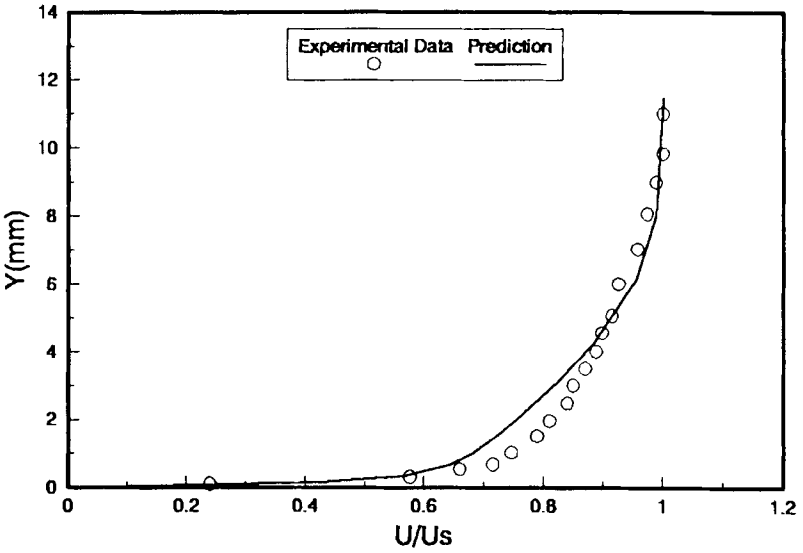

Figure 12. Average velocity profile (0°) (case B)

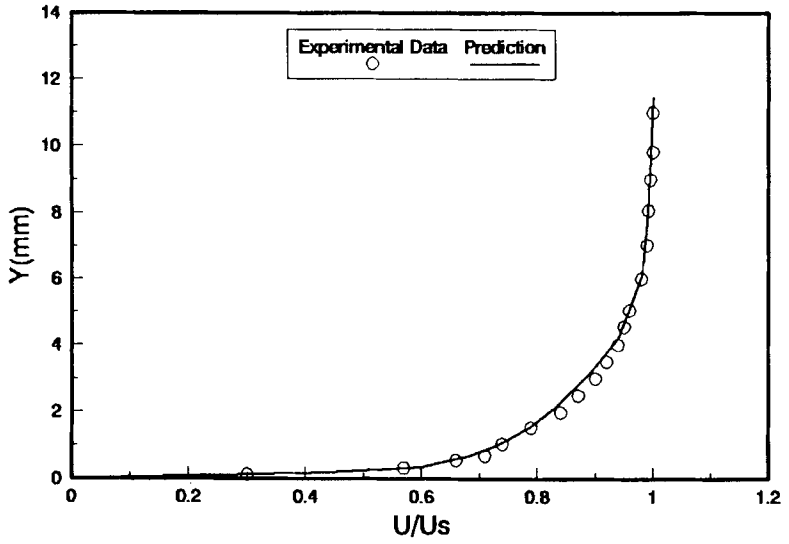

Figure 13. Average velocity profile (90°) (case B)

How this modelling should change with amplitude and frequency is still an unexplored question. On the other hand, the phase-frozen velocity profiles discussed in the next paragraph are remarkably good.

In Figures 12–15 the average velocity profiles for the given phases during one cycle are presented as functions of the distance normal to the wall. The velocity is reduced by its value u_s at

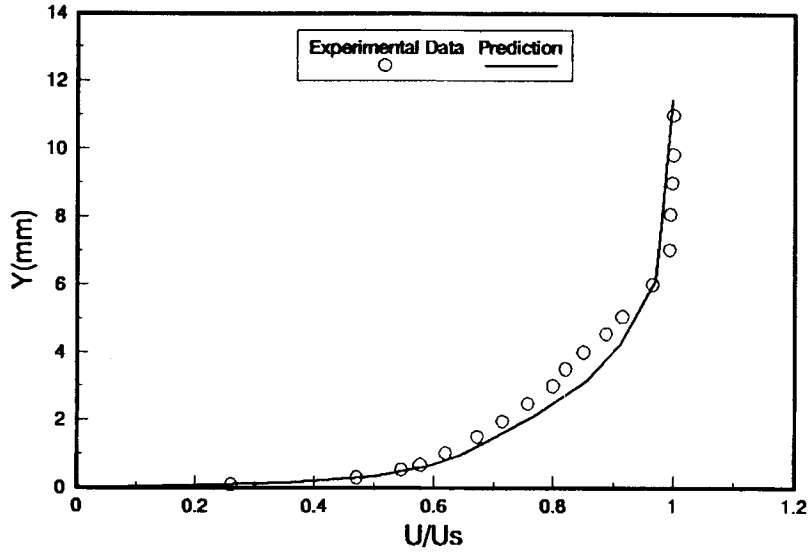

Figure 14. Average velocity profile (180°) (case B)

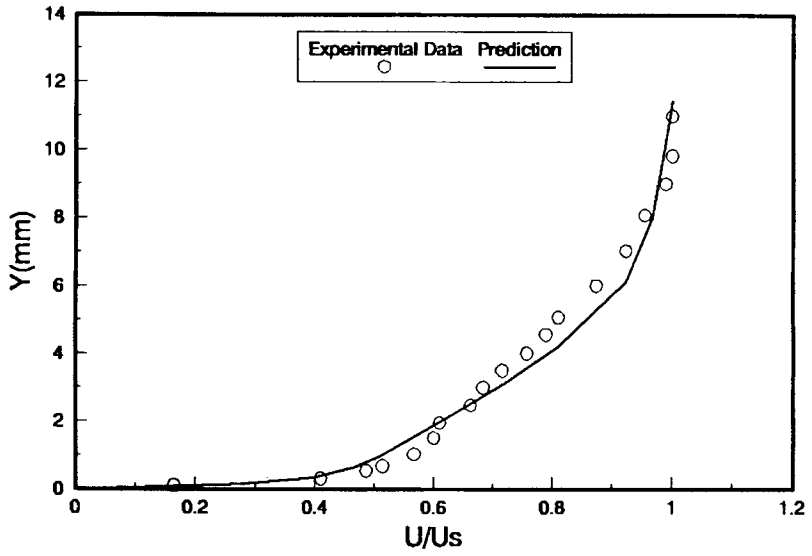

Figure 15. Average velocity profile (270°) (case B)

the symmetry line for the same value of the phase angle. It is seen that the experimental profiles are reasonably well reproduced.

5. CONCLUDING REMARKS

The present numerical study of a turbulent channel flow which is developing in the presence of a small oscillation appears to agree with the previous experimental observation that the general

behaviour of the flow and the structure of the turbulence are not fundamentally affected by the unsteadiness of the flow.

The numerical calculations show that the present method is effective for the prediction of periodically oscillating turbulent flows. The predictions for the flow configurations considered here agreed satisfactorily with the experimental data. The method of averaging appears to work well and results in a significant reduction in computer time.

The Baldwin–Lomax eddy viscosity model seems to work well for unsteady as well as steady flow, at least for conditions similar to those of the present study. Further numerical experiments for separated flows are currently under way.

Further work is needed to develop modifications to the turbulence model to 'unfreeze' the eddy viscosity to account for large relative amplitudes of the periodic component, and the effect of frequency needs to be investigated.

ACKNOWLEDGEMENTS

This work has been supported by the Canadian Natural Sciences and Engineering Research Council.

APPENDIX: NOMENCLATURE

$\mathbf{A}$	mean component of nodal vector of unknowns
$\mathbf{B}, \mathbf{C}$	in-phase and out-of-phase amplitudes of periodic component of nodal vector of unknowns
$\mathbf{d}$	nodal vector of unknowns
D	Van Driest damping factor
f	frequency (cycles per second)
h	half-channel width (Figure 1)
$\mathbf{K}$	stiffness matrix
L	length of calculation domain (Figure 1)
$\mathbf{M}$	mass matrix
M_i, N_i	finite element shape functions
p	pressure
Re	$u_c \rho h/\mu$, Reynolds number
St	$\Omega h/u_c$, Strouhal number
t	time
u, v	velocity components in x, y
u_m	mean component of velocity
u_p	harmonic component of velocity
u_s	velocity at symmetry line
u_0	inlet velocity
u_c	inlet mean velocity at symmetry line
A_c	inlet amplitude at symmetry line
x, y	co-ordinates (Figure 1)
u^+	$u_m/\sqrt{(\rho/\tau_w)}$
y^+	$\sqrt{(\rho\tau_w)}y/\mu$
δ_1	boundary layer displacement thickness
μ	molecular viscosity
μ_e	$\mu_t + \mu$ effective viscosity
μ_t	eddy viscosity

ρ	density
τ	shear stress
τ_w	wall shear stress
ϕ	phase angle
ω	vorticity
Ω	$2\pi f$

REFERENCES

1. S. K. F. Karlsson, 'An unsteady turbulent boundary layer', *J. Fluid Mech.*, **5**, 622–636 (1959).
2. J. Cousteix, A. Desopper and R. Houdeville, 'Structure and development of a turbulent boundary layer in an oscillatory external flow', in *Turbulent Shear Flows I*, 1977, pp. 154–171. Springer-Verlag, Berlin/Heidelberg/New York.
3. G. Binder and J. L. Kueny, 'Measurements of the periodic velocity oscillations near the wall in unsteady turbulent channel flow', *Unsteady Turbulent Shear Flow, IUTAM Symp.*, 1981, pp. 100–108. Springer-Verlag, Berlin/Heidelberg/New York.
4. L. W. Carr, 'A compilation of unsteady turbulent boundary layer experimental data', *AGARD-AG-265*, 1981.
5. D. P. Telionis and D. Th. Tsahalis, 'Unsteady turbulent boundary layers and separation', *AIAA J.*, **14**, 468–474 (1976).
6. D. P. Telionis, Review — unsteady boundary layers, separated and attached, *J. Fluids Eng.*, **101**, 29–43 (1979).
7. J. Cousteix and R. Houdeville, 'Response of a turbulent boundary layer to a pulsation of the external flow with and without adverse pressure gradient', *Unsteady Turbulent Shear Flows, IUTAM Symp.*, 1981, pp. 120–144. Springer-Verlag, Berlin/Heidelberg/New York.
8. P. R. Spalart and B. S. Baldwin, 'Direct simulation of a turbulent oscillating boundary layer', in *Turbulent Shear Flows 6*, 1989, pp. 417–440. Springer-Verlag, Berlin/Heidelberg.
9. P. G. Pattani and M. D. Olson, 'Periodic solutions of rigid body–viscous flow interaction', *Int. j. numer. methods fluids*, **7**, 653–695 (1987).
10. M. D. Olson and Z. Qin, 'A finite element algebraic closure model for turbulent separated–reattaching flows', *Commun. Appl. Numer. Methods*, **5**, 435–442 (1989).
11. B. S. Baldwin and H. Lomax, 'Thin layer approximation and algebraic model for separated turbulent flows', *AIAA Paper 78-257*, 1978.
12. P. G. Pattani and M. D. Olson, 'Finite element–algebraic closure modelling of turbulent entrance type flows', *5th Int. Conf. on Laminar and Turbulent Flows*, 1987, pp. 386–397. Pineridge Press, Swansea, U.K.
13. Z. Qin and M. D. Olson, 'Finite element–algebraic closure analysis of turbulent separated–reattaching flow around a rectangular body', *Comput. Methods Appl. Mech. Eng.*, **85**, 131–150 (1991).